

Monte Carlo study of the isotropic–nematic interface in suspensions of spherocylinders

Tanja Schilling¹, Richard Vink¹, and Stefan Wolfsheimer¹

Johannes Gutenberg Universität Mainz, 55099 Mainz, Germany

Abstract. The isotropic to nematic transition in suspensions of anisotropic colloids is studied by means of grand canonical Monte Carlo simulation. From measurements of the grand canonical probability distribution of the particle density, the coexistence densities of the isotropic and the nematic phase are determined, as well as the interfacial tension.

1 Introduction

On change of density, suspensions of rod-like particles undergo a phase transition between an isotropic fluid phase, where the particle orientations are evenly distributed, and an anisotropic fluid phase (called “nematic” phase), where the particle orientations are on average aligned. Fig. 1 shows a sketch of these phases.

In the 1940s, this phenomenon was explained by Lars Onsager in a theory based on infinitely elongated hard spherocylinders [1]. Onsager showed that the basic mechanism of the transition is the interplay between positional and orientational entropy. The size of the excluded volume – i.e. the volume around one particle, which another particle cannot enter, because it would produce an overlap – depends on the angle between the two particles’ axis. If the particles lie parallel, the excluded volume is minimized. Hence particles which are aligned, gain accessible volume and therefore positional entropy, but they lose orientational entropy. At a certain density the balance between

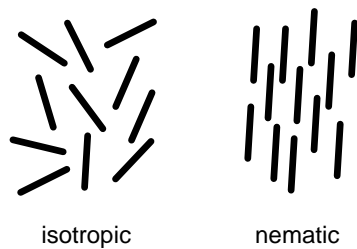


Fig. 1. Sketches of the isotropic phase (left) and nematic phase (right): In the isotropic phase, particle positions and orientations are disordered. In the nematic phase, particle orientations are aligned.

the two contributions flips and the system changes from the isotropic to the nematic phase.

Onsager theory has been remarkably successful at describing the isotropic to nematic (IN) transition, and still serves as the basis for many theoretical investigations of the properties of liquid crystals. Over the last twenty years, for instance, several groups have investigated the properties of the interface between the two phases using Onsager-type density functional approaches [2–8].

The IN interface is an interesting model system, because both phases are almost incompressible and their densities are similar. Therefore pressure and density are not important parameters. The only parameters which determine the properties of the interface are the particle aspect ratio and the orientation of the director (i.e. the axis of average orientation of the particles in the nematic phase) with respect to the plane of the interface.

An important finding of the theoretical studies cited above is that the interfacial tension γ_{IN} of the IN interface is minimized when the director lies in the plane of the interface. In this case γ_{IN} is predicted to be very low, but the precise value varies considerably between different authors [9,10]. Theoretical estimates for γ_{IN} typically range from 0.156 [7] to 0.34 [3], in units of $k_B T/LD$, with L the rod length, D the rod diameter, T the temperature, and k_B the Boltzmann constant.

To test the accuracy of the theoretical estimates of γ_{IN} , one might wish to make a direct comparison to experimental data. Unfortunately, this is not straightforward. The models used in theoretical treatments of the IN interface are typically rather simplistic, usually based on a hard or short-ranged pair potential in a system of monodisperse spherocylinders. Using these models, it is not reasonable to expect quantitative agreement with experiments, because the interactions in the experimental system will be much more complex. For example, polydispersity may be an important factor, and it is not clear to what extent long-range interactions play a role. Also many experimental systems display chirality. And even the experimental determination of the rod dimensions L and D , required if a comparison to theory is to be made, presents complications [10].

In order to validate the assumptions made by the various approaches, it is nevertheless important to test the accuracy of the theoretical predictions. To this end, computer simulations are ideal, because they, in principle, probe the phase behavior of the model system without resorting to approximations. In recent years, several groups have investigated the IN transition by means of simulations [11–18]. However, the interfacial tension γ_{IN} was not measured in these studies.

To obtain γ_{IN} in simulations rather elaborate simulation techniques are required. One possibility is to measure the anisotropy of the pressure tensor.

The interfacial tension is obtained from the difference between the normal and the transversal pressure tensor components:

$$\gamma_{IN} = \int_{-\infty}^{\infty} P_N(z) - P_T(z) dz, \quad (1)$$

where the interface lies in the xy -plane. In [18], this method is applied to suspensions of ellipsoids with axial ratio $\kappa = A/B = 15$, where A is the length of the symmetry axis, and B that of the transverse axis. The measured interfacial tension is $0.006 \pm 0.005 k_B T/B^2 \approx 0.09 k_B T/AB$ if a hard interaction potential is used, and $0.011 \pm 0.004 k_B T/B^2 \approx 0.165 k_B T/AB$ for a soft potential. The anisotropy of the pressure tensor is very small, and thus difficult to measure accurately. Therefore the error bars of these results are large.

Another approach is via the capillary wave spectrum. The basic idea is the following: the interface will fluctuate for entropic reasons. As enlargement of the interfacial area costs energy, the spectrum of the fluctuations is related to γ_{IN} . If the interface is described by a function $h(x, y)$, then one can show that

$$\langle |h(\mathbf{q})|^2 \rangle = \frac{k_B T}{\gamma_{IN} q^2}, \quad (2)$$

where $h(\mathbf{q})$ is the Fourier transformed of $h(x, y)$ [19]. In [19] this approach was applied to soft ellipsoids with $\kappa = 15$. $\gamma_{IN} = 0.016 \pm 0.002 k_B T/B^2 \approx 0.24 k_B T/AB$ is reported. However, capillary wave theory is only valid in the long wavelength limit. Therefore very large system sizes are required. Moreover, if periodic boundary conditions are used, two interfaces will be present in the simulation box. Since γ_{IN} is very small, large capillary fluctuations can occur, and one needs to be aware of interactions between the two interfaces. Therefore this method requires very large system sizes.

Clearly, in order to obtain γ_{IN} more accurately, much more computer power or different simulation techniques are required. In this article we present a method, which allows to reduce statistical errors considerably and therefore makes an analysis of the finite-size effects possible. Recent advances in grand canonical sampling methods [20,21] have enabled accurate measurements of the interfacial tension in simple fluids [22,23] and colloid–polymer suspensions [24,25]. The aim of this paper is to apply these techniques to the IN transition in a system of soft spherocylinders, and to extract the corresponding phase diagram and the interfacial tension. Simulations in the grand canonical ensemble offer a number of advantages over the more conventional methods discussed previously. More precisely, in grand canonical simulations, both the coexistence properties can be probed, as well as the interfacial properties – where as the methods described above require an independent estimate of the coexistence densities. Additionally, finite–size scaling methods are available which can be used to extrapolate simulation data to the thermodynamic limit [26–29].

This article is structured as follows: First, we introduce the soft spherocylinder model used in this work. Next, we describe the grand canonical Monte Carlo method, and explain how the coexistence properties, and the interfacial tension are obtained. Finally, we present our results.

2 Model

For numerical reasons, which will be explained in Sect. 3, we do not model the particles as hard rods, but as repulsive soft rods. Two spherocylinders of elongation L and diameter D interact via a pair potential of the form

$$V(\mathbf{r}_1, \mathbf{r}_2, \mathbf{u}_1, \mathbf{u}_2) = \begin{cases} \epsilon & : r < D \\ 0 & : \text{otherwise} \end{cases}, \quad (3)$$

where \mathbf{r}_1 , \mathbf{r}_2 , \mathbf{u}_1 and \mathbf{u}_2 are defined in Fig. 2 and r is the distance between the particles' axis. The total energy is thus proportional to the number of overlaps in the system. In this article, the rod diameter D is taken as unit of length, and $k_B T$ as unit of energy. The strength of the potential is set to $\epsilon = 2 k_B T$. Note that in the limit $\epsilon \rightarrow \infty$, this model approaches a system of infinitely hard rods. The effect of the particle softness is only a shift in the coexistence densities to higher values. The transition mechanism remains the same.

To study the IN transition, we use the density and the rod alignment as order parameters. Both the isotropic and the nematic phase are fluid phases, in the sense that long-range positional order of the centers of mass is absent. Orientational order is measured by the S_2 order parameter, defined as the maximum eigenvalue of the thermal average of the orientational tensor \underline{Q} :

$$Q_{\alpha\beta} = \frac{1}{2N} \sum_{i=1}^N (3u_{i\alpha}u_{i\beta} - \delta_{\alpha\beta}). \quad (4)$$

Here, $u_{i\alpha}$ is the α component ($\alpha = x, y, z$) of the orientation vector \mathbf{u}_i of rod i (normalized to unity), and $\delta_{\alpha\beta}$ is the Kronecker delta. In the case of orientational order S_2 assumes a value close to one, while in the disordered isotropic phase, S_2 is close to zero.

Since the density of the nematic phase is slightly higher than that of the isotropic phase, we may also use the particle number density $\rho = N/V$ to

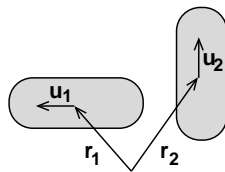


Fig. 2. Definition of the quantities used in eqn. 3

distinguish between the phases, with N the number of rods in the system, and V the volume of the simulation box. Following convention, we also introduce the reduced density $\rho^* = \rho/\rho_{cp}$, with $\rho_{cp} = 2/(\sqrt{2} + (L/D)\sqrt{3})$ the density of regular close packing of hard spherocylinders.

3 Simulation method

The simulations are performed in the grand canonical ensemble. In this ensemble, the volume V , the temperature T , and the chemical potential μ of the rods are fixed, while the number of rods N inside the simulation box fluctuates. Insertion and removal of rods are attempted with equal probability, and accepted with the standard grand canonical Metropolis rules, given by

$$A(N \rightarrow N + 1) = \min \left[1, \frac{V}{N + 1} \exp(-\beta\Delta E + \beta\mu) \right] \quad (5)$$

and

$$A(N \rightarrow N - 1) = \min \left[1, \frac{N}{V} \exp(-\beta\Delta E - \beta\mu) \right], \quad (6)$$

where ΔE is the energy difference between initial and final state, and $\beta = 1/k_B T$ [27,30]. Here it becomes evident, why this method is difficult to apply to a system of hard objects – insertion moves will become extremely unlikely, if overlaps are forbidden. Therefore we introduced a finite energy cost instead.

The simulations are performed in a three dimensional box of size $L_x \times L_y \times L_z$ using periodic boundary conditions in all directions. In this work, we fix $L_x = L_y$, but we allow for elongation $L_z \geq L_x$. Moreover, to avoid double interactions between rods through the periodic boundaries, we set $L_x > 2L$.

During the simulations, we measure the probability distribution $P(N)$, defined as the probability of observing a system containing N rods. The shape of the distribution will depend on the following parameters:

- the aspect ratio L/D
- the temperature T (in a trivial way, because it just sets the energy scale.)
- the chemical potential μ
- the box dimensions L_x and L_z , because there will be finite-size effects.

At phase coexistence, the distribution $P(N)$ becomes bimodal, with two peaks of equal area, one located at small values of N corresponding to the isotropic phase, and one located at high values of N corresponding to the nematic phase. A typical coexistence distribution is shown in Fig. 3, where the logarithm of $P(N)$ is plotted.

In order to find the chemical potential of coexistence, we use the equal area rule [31]. Coexistence is defined as the situation in which the areas under the peaks are equal:

$$\int_0^{\langle N \rangle} P(N) dN = \int_{\langle N \rangle}^{\infty} P(N) dN, \quad (7)$$

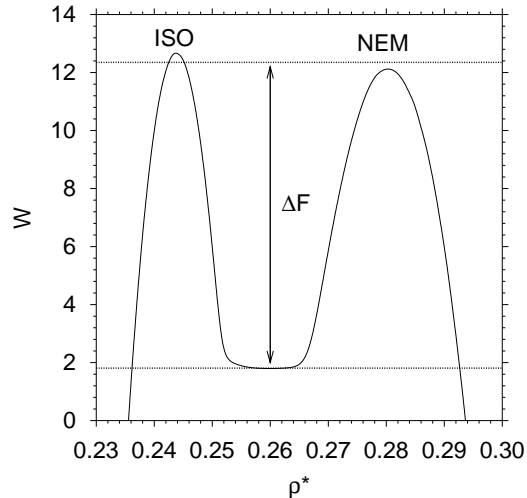


Fig. 3. Coexistence distribution $W = k_B T \ln P(N)$ of the isotropic to nematic transition in a system of soft rods with $\epsilon = 2$ and $L/D = 15$. The low density peak corresponds to the isotropic phase (ISO), the high density peak to the nematic phase (NEM), and the barrier ΔF to the free energy difference between the two phases (ΔF is given by the average peak height as measured from the minimum in between the peaks). The above distribution was obtained using box dimensions $L_x = 2.1L$ and $L_z = 8.4L$.

where $\langle N \rangle$ is the average of the full distribution

$$\langle N \rangle = \int_0^\infty N P(N) dN, \quad (8)$$

and we assume that $P(N)$ has been normalized to unity $\int_0^\infty P(N) dN = 1$. The coexistence density of the isotropic phase follows trivially from the average of $P(N)$ in first peak

$$\rho_{\text{iso}} = (2/V) \int_0^{\langle N \rangle} N P(N) dN, \quad (9)$$

and similarly for the nematic phase

$$\rho_{\text{nem}} = (2/V) \int_{\langle N \rangle}^\infty N P(N) dN, \quad (10)$$

where the factors of two are a consequence of the normalization of $P(N)$.

The interfacial tension γ_{IN} is extracted from the logarithm of the probability distribution $W \equiv k_B T \ln P(N)$. Since $-W$ corresponds to the free energy of the system, the average height ΔF of the peaks in W , measured

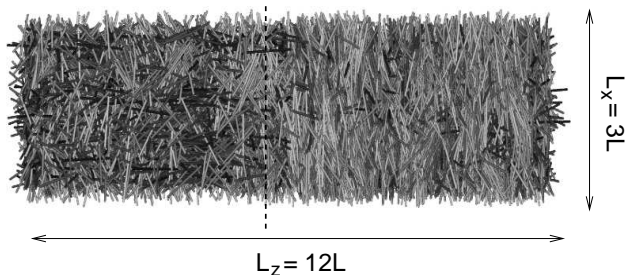


Fig. 4. Snapshot of a system of soft spherocylinders at IN coexistence. The spherocylinders are shaded according to their orientation. On the left side of the dashed line the system is isotropic, on the right side it is nematic. The second interface coincides with the boundaries of the box in the elongated direction.

with respect to the minimum in between the peaks, equals the free energy barrier separating the isotropic from the nematic phase. Which configurations contribute to $P(N)$ in the region where the overall density of the system is between the peaks $\rho_{\text{iso}} \ll \rho \ll \rho_{\text{nem}}$? A snapshot of the system in this regime (Fig. 4) reveals a slab geometry, with one isotropic region, and one nematic region, separated by an interface (because of the periodic boundary conditions, there are actually two interfaces). Note that the director of the nematic phase lies in the plane of the interfaces. This was the typical case for the snapshots studied by us, and is consistent with the theoretical prediction that in-plane alignment yields the lowest free energy. From this snapshot it becomes evident why the distribution has a flat region. If the two interfaces are sufficiently separated they do not interact. Then it is possible to change the overall system density simply by growing one phase and shrinking the other without producing any free energy.

The barrier ΔF in Fig. 3 thus corresponds to the free energy cost of creating two interfaces in the system. In this work, where the box dimensions are chosen such that $L_x = L_y$ and $L_z \geq L_x$, the interfaces will be oriented perpendicular to the elongated direction, since this minimizes the interfacial area, and hence the free energy of the system. The total interfacial area in the system thus equals $2L_x^2$. As the interfacial tension is simply the excess free energy per unit area, we may write

$$\gamma_{IN}(L_x) = \Delta F / (2L_x^2), \quad (11)$$

with $\gamma_{IN}(L_x)$ the interfacial tension in a finite simulation box with lateral dimension L_x [26].

To obtain the interfacial tension in the thermodynamic limit, one can perform a finite size scaling analysis [26] to estimate $\lim_{L_x \rightarrow \infty} \gamma_{IN}(L_x)$. Alternatively, away from any critical point, the most dominant finite size effects will likely stem from interactions between the two interfaces. In this case, it is feasible to use an elongated simulation box with $L_z \gg L_x$, such as in Fig. 4.

This article is intended as an introduction to the simulation method. Therefore we will focus on the second aspect. A finite size analysis of our results can be found in [32].

If the free energy barrier ΔF is large, transitions between the isotropic and the nematic phase become less likely, and the simulation will spend most of the time in only one of the two phases. A crucial ingredient in our simulation is therefore the use of a biased sampling technique. We use successive umbrella sampling [21] to enable accurate sampling in regions where $P(N)$, due to the free energy barrier separating the phases, is very small. Note also that phase coexistence is only observed if the chemical potential μ is set equal to its coexistence value. This value is in general not known at the start of the simulation, but it may easily be obtained by using the equation $P(N|\mu_1) = P(N|\mu_0)e^{\beta(\mu_1-\mu_0)N}$, with $P(N|\mu_\alpha)$ the probability distribution $P(N)$ at chemical potential μ_α . In the simulations, we typically set the chemical potential to zero and use successive umbrella sampling to obtain the corresponding probability distribution. We then use the above equation to obtain the desired coexistence distribution, in which the area under both peaks is equal.

4 Results

4.1 Profiles

First we estimated the minimum box size necessary to contain two independent interfaces. We ran an NVT Monte Carlo simulation of hard spherocylinders at coexistence in a very elongated box ($L_z = 10L$) and measured the interfacial width. Fig. 5 shows the density (top) and the nematic order parameter (bottom) perpendicular to the interface. We do not see any trace of non-monotonous behaviour. In agreement with Onsager theory, the interfaces are shifted with respect to one another. Moving from the nematic to the isotropic region, first ρ drops and then S_2 . Measured from the point where the density is $0.9\rho_{\text{iso}}$ to the point, where it is $0.9\rho_{\text{nem}}$ the interface is roughly $4L$ wide. This means that very large simulation boxes will be necessary to properly decouple two interfaces.

4.2 Phase diagram

First we used our grand canonical Monte Carlo scheme to determine the IN phase diagram of the soft spherocylinder system of eqn. 3 using $\epsilon = 2$. For several rod elongations L/D , we measured the distribution $P(N)$, from which ρ_{iso} and ρ_{nem} were obtained. The system size used in these simulations is typically $L_x = L_y = 2.1L$ and $L_z = 4.2L$. In Fig. 6, we plot the reduced density of the isotropic and the nematic phase as function of L/D . We observe that the phase diagram is qualitatively similar to that of hard spherocylinders

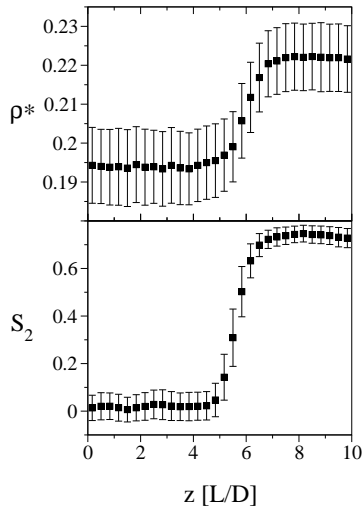


Fig. 5. Profiles of density and nematic order perpendicular to the interface for $L/D = 15$. In agreement to Onsager theory, the profiles are shifted by roughly $0.3 L/D$ with respect to one another.

[12]. The quantitative difference being that, for soft rods, the IN transition is shifted towards higher density. The inset of Fig. 6 shows the concentration variable $c = \pi D L^2 \rho / 4$ as a function of D/L . For hard spherocylinders, Onsager theory predicts that $c_{\text{ISO}} = 3.29$ and $c_{\text{NEM}} = 4.19$ in the limit of infinite rod length, or equivalently $D/L \rightarrow 0$. In case of the soft potential of eqn. 3, these values must be multiplied by $(1 - e^{-\beta\epsilon})^{-1} \approx 1.16$ for $\epsilon = 2$. In the inset of Fig. 6, the corresponding limits are marked with arrows. As in [12], we observe that the simulation data for the isotropic phase smoothly approach the Onsager limit, while the nematic branch of the binodal seems to overshoot the Onsager limit. This we attribute to equilibration problems. To simulate the IN transition in the limit $D/L \rightarrow 0$, large system sizes are required, and it becomes increasingly difficult to obtain accurate results. To quantify the uncertainty in our measurements, additional independent simulations for rod elongation $L/D = 25, 30,$ and 35 were performed. The corresponding data are also shown in Fig. 6. For $L/D \geq 30$, we observe significant scatter, while for $L/D \leq 25$, the uncertainty is typically smaller than the symbol size used in the plots.

4.3 Interfacial tension

Next, the interfacial tension γ_{IN} is determined for $L/D = 10$ and $L/D = 15$. Unfortunately, the system size used to compute the phase diagram in the previous section, was insufficient to accurately extract the interfacial tension

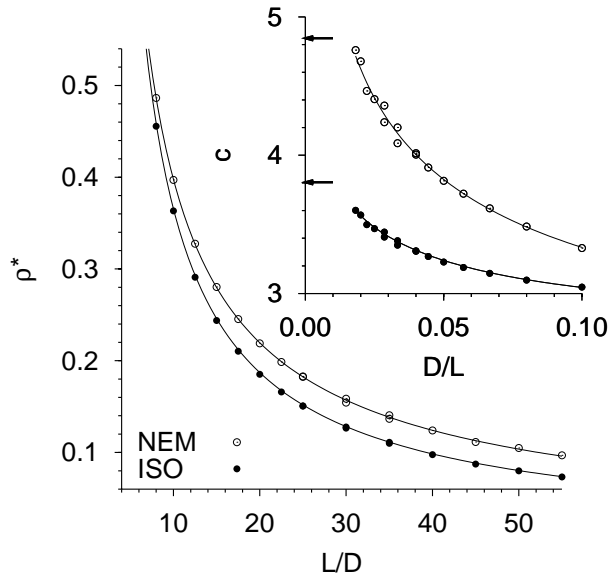


Fig. 6. Soft spherocylinder phase diagram of the IN transition using $\epsilon = 2$. Shown is the reduced density ρ^* of the isotropic phase (closed circles) and of the nematic phase (open circles) as function of L/D . The inset shows the concentration variable c as function of D/L for both the isotropic and the nematic phase. The lower and upper arrow in the inset mark the Onsager limit $D/L \rightarrow 0$ for the isotropic and the nematic phase, respectively. The lines connecting the points serve as a guide to the eye.

because no flat region between the peaks in $P(N)$ could be distinguished. To properly extract the interfacial tension, much larger systems turned out to be required. In this case, care must be taken in the sampling procedure. Many sampling schemes, especially the ones that are easy to implement such as successive umbrella sampling, put a bias on the density only. Such schemes tend to “get stuck” in meta-stable droplet states when the system size becomes large [24]. As a result, one may have difficulty reaching the state with two parallel interfaces, in which case eqn. 11 cannot be used.

Therefore, for large systems, one must carefully check the validity of the simulation results. We performed a number of additional grand canonical simulations using a biased Hamiltonian of the form $\mathcal{H} = \mathcal{H}_0 + W$, with \mathcal{H}_0 the Hamiltonian of the real system defined by eqn. 3 and $W = -k_B T \ln P(N)$. If the measured $P(N)$ is indeed the equilibrium coexistence distribution of the real system, a simulation using the biased Hamiltonian should visit the isotropic and the nematic phase equally often on average [33,24]. This is illustrated in the top frame of Fig. 7, which shows the S_2 order parameter as a function of the elapsed simulation time during one such biased simulation.

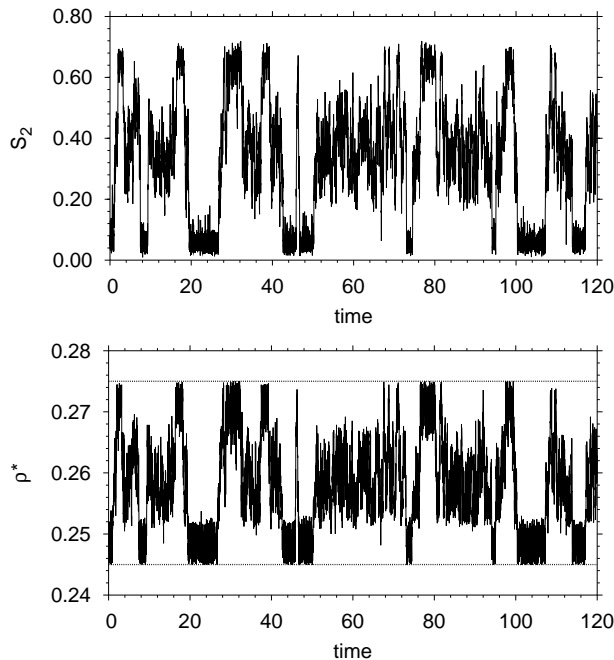


Fig. 7. Monte Carlo time series of a biased grand canonical simulation. The top frame shows the S_2 order parameter as a function of the invested CPU time, the lower frame the reduced density, with CPU time expressed in hours on a 2.6 GHz Pentium. During the simulation, the reduced density was confined to the interval $0.245 < \rho^* < 0.275$, as indicated by the horizontal lines in the lower figure. The data were obtained using $L/D = 15$, $\epsilon = 2$, $L_x = 2.1L$ and $L_z = 8.4L$, which are the same parameters as used in Fig. 3.

Indeed, we observe frequent transitions between the isotropic ($S_2 \sim 0$) and the nematic phase ($S_2 \sim 1$). Also shown in Fig. 7 is the corresponding time series of the reduced density. In case that a perfect estimate for $P(N)$ could be provided, the measured distribution in the biased simulation will become flat in the limit of long simulation time. The deviation from a flat distribution can be used to estimate the error in $P(N)$, or alternatively, to construct a better estimate for $P(N)$. The latter approach was adopted by us. First, successive umbrella sampling is used to obtain an initial estimate for $P(N)$. This estimate is then used as input for a number of biased simulations using the modified Hamiltonian, and improved iteratively each time.

To obtain the interfacial tension, the most straightforward approach is to fix the lateral box dimensions at $L_x = L_y$, and to increase the elongated dimension $L_z \gg L_x$ until a flat region between the peaks in the distribution $P(N)$ appears. For soft spherocylinders of elongation $L/D = 10$, the results of

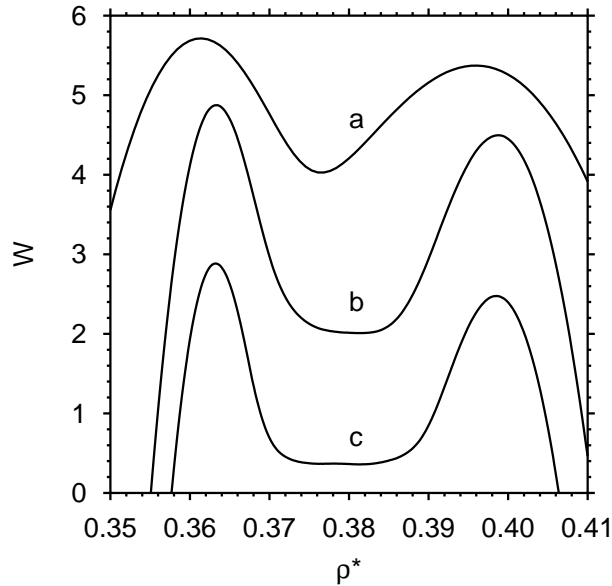


Fig. 8. Coexistence distributions $W = k_B T \ln P(N)$ of soft spherocylinders with $L/D = 10$ and $\epsilon = 2$ for various system sizes. In each of the above distributions, the lateral box dimension was fixed at $L_x = L_y = 2.3L$, while the perpendicular dimension was varied: (a) $L_z = 2.3L$; (b) $L_z = 10.35L$; (c) $L_z = 13.8L$. The corresponding free energy barriers ΔF are: (a) 1.52; (b) 2.68; (c) 2.33, in units of $k_B T$.

this procedure are shown in Fig. 8. Indeed, we observe that the region between the peaks becomes flatter as the elongation of the simulation box is increased. Unfortunately, even for the largest system that we could handle, the region between the peaks still displays some curvature. In other words, the interfaces are still interacting, indicating that even more extreme box elongations are required. Ignoring this effect, and applying eqn. 11 to the largest system of Fig. 8, we obtain for the interfacial tension $\gamma_{IN} = 0.0022 k_B T/D^2$. For rod elongation $L/D = 15$, the distribution of the largest system that we could handle is shown in Fig. 3. The height of the barrier reads $\Delta F = 10.59 k_B T$, and the corresponding interfacial tension $\gamma_{IN} = 0.0053 k_B T/D^2$.

The advantage of the present simulation approach is that the statistical errors are small, and that finite size effects are clearly visible as a result. In contrast, if the pressure tensor or capillary broadening are used to obtain γ_{IN} , the statistical errors will likely obscure any finite size dependence.

Table 1. Bulk properties of the coexisting isotropic and nematic phase in a system of soft spherocylinders with $\epsilon = 2$ and $L/D = 10$ and 15. Listed are the reduced density ρ^* of the isotropic and the nematic phase, the normalized number density ρLD^2 and the interfacial tension γ_{IN} , expressed in two types units to facilitate the comparison to other work.

L/D	isotropic phase		nematic phase		interfacial tension γ_{IN}	
	ρ^*	ρLD^2	ρ^*	ρLD^2	$\frac{k_B T}{D^2}$	$\frac{k_B T}{LD}$
10	0.363	0.388	0.397	0.424	0.0022 ± 0.0003	0.033
15	0.244	0.267	0.280	0.307	0.0053 ± 0.0001	0.080

5 Discussion

It is clear from the phase diagram of Fig. 6 that the Onsager limit is not recovered until for very large rod elongation, exceeding at least $L/D = 40$. As a result, our estimates for the interfacial tension differ profoundly from Onsager predictions. Typically, γ_{IN} in our simulations is four times lower than Onsager estimates. Note that our simulations also show that γ_{IN} increases with L/D , towards the Onsager result, so there seems to be qualitative agreement. However, to properly access the Onsager regime, additional simulations for large elongation L/D are required. Unfortunately, as indicated by the scatter in the data of Fig. 6, and also in [12], such simulations are very complicated. It is questionable if present simulation techniques are sufficiently powerful to extract γ_{IN} with any meaningful accuracy in the Onsager regime.

As mentioned in the introduction, computer simulations of soft ellipsoids with $\kappa = 15$ yield interfacial tensions of $\gamma_{IN} = 0.011 \pm 0.004 k_B T/B^2$ and $\gamma_{IN} = 0.016 \pm 0.002 k_B T/B^2$ [18,19]. For $L/D = 15$, our result for soft spherocylinders is considerably lower. Obviously, spherocylinders are not ellipsoids, and this may well be the source of the discrepancy. Note also that the shape of the potential used by us is different from that of Refs. [18,19].

In summary, we have performed grand canonical Monte Carlo simulations of the IN transition in a system of soft spherocylinders. By measuring the grand canonical order parameter distribution, the coexistence densities as well as the interfacial tension were obtained. In agreement with theoretical expectations and other simulations, ultra-low values for the interfacial tension γ_{IN} are found. Our results confirm that for short rods, the interfacial tension, as well as the coexistence densities, are considerably lower than the Onsager predictions. This demonstrates the need for improved theory to describe the limit of shorter rods, which is required if the connection to experiments is ever to be made.

5.1 Acknowledgement

We are grateful to the Deutsche Forschungsgemeinschaft (DFG) for support (TR6/A5) and to K. Binder, M. Müller, P. van der Schoot, and R. van Roij

for stimulating discussions. We also thank G. T. Barkema for suggesting some of the numerical optimizations used in this work. T. S. was supported by the Emmy Noether program of the DFG.

References

1. L. Onsager: *Ann. N. Y. Acad. Sci.* **51**, 627 (1949)
2. M. Doi, N. Kuzuu: *Appl. Polym. Symp.* **41**, 65 (1985)
3. W.E. McMullen: *Phys. Rev. A* **38**, 6384 (1988)
4. Z.Y. Chen, J. Noolandi: *Phys. Rev. A* **45**, 2389 (1992)
5. Z.Y. Chen: *Phys. Rev. E* **47**, 3765 (1993)
6. D.L. Koch, O.G. Harlen: *Macromolecules* **32**, 219 (1999)
7. K. Shundyak, R. van Roij: *J. Phys.: Condens. Matter* **13**, 4789 (2001)
8. E. Velasco, L. Mederos, D.E. Sullivan: *Phys. Rev. E* **66**, 021708 (2002)
9. P. van der Schoot: *J. Phys. Chem. B* **103**, 8804 (1999)
10. W. Chen, D.G. Gray: *Langmuir* **18**, 663 (2002)
11. M. Dijkstra, R. van Roij, R. Evans: *Phys. Rev. E* **63**, 051703 (2001)
12. P. Bolhuis, D. Frenkel: *J. Chem. Phys.* **106**, 666 (1997)
13. M.A. Bates, C. Zannoni: *Chem. Phys. Lett.* **280**, 40 (1997)
14. M.A. Bates, C. Zannoni: *Chem. Phys. Lett.* **288**, 209 (1998)
15. M.P. Allen: *J. Chem. Phys.* **112**, 5447 (2000)
16. M.P. Allen: *Chem. Phys. Lett.* **331**, 513 (2000)
17. M.S. Al-Barwani, M.P. Allen: *Phys. Rev. E* **62**, 6706 (2000)
18. A.J. McDonald, M.P. Allen, F. Schmid: *Phys. Rev. E* **63**, 010701 (2000)
19. N. Akino, F. Schmid, M.P. Allen: *Phys. Rev. E* **63**, 041706 (2001)
20. Q. Yan, J.J. de Pablo, J. Chem. Phys. **113**, 1276 (2000)
21. P. Virnau, M. Müller: *J. Chem. Phys.* **120**, 10925 (2004)
22. J. Potoff, A. Panagiotopoulos: *J. Chem. Phys.* **112**, 6411 (2000)
23. W. Gózdź: *J. Chem. Phys.* **119**, 3309 (2003)
24. P. Virnau, M. Müller, L.G. MacDowell, K. Binder: *J. Chem. Phys.* **121**, 2169 (2004)
25. R.L.C. Vink, J. Horbach: *J. Chem. Phys.* **121**, 3253 (2004)
26. K. Binder: *Phys. Rev. A* **25**, 1699 (1982)
27. D.P. Landau, K. Binder: *A Guide to Monte Carlo Simulations in Statistical Physics* (Cambridge University Press, Cambridge, 2000)
28. A.D. Bruce, N.B. Wilding: *Phys. Rev. Lett.* **68**, 193 (1992)
29. Y.C. Kim, M.E. Fisher, E. Luijten: *Phys. Rev. Lett.* **91**, 065701 (2003)
30. D. Frenkel, B. Smit: *Understanding Molecular Simulation* (Academic Press, San Diego, 2001)
31. M. Müller, N.B. Wilding: *Phys. Rev. E* **51**, 2079 (1995)
32. R. Vink, T. Schilling: *cond-mat/0502444* (2005)
33. N.B. Wilding: *Am. J. Phys.* **69**, 10 (2001)